Iran J Orthod. 2026 June; 21(1):e1413. doi:10.22034/ijo.2026.2087236.1413.
Published online 2026 June 1 Research Article
Original Article **Open Access**

Stress Distribution During Infra Zygomatic Crest-Supported Full-Arch Distalization with Intrusion Using Single and Dual TAD Configurations: A Finite Element Study

Sandeep Shetty [1], Adil Mohamed Ashraf [2], Dilshad Umar [3]*

[1] Professor, Department of Orthodontics and Dentofacial Orthopaedics, Yenepoya Dental College, Yenepoya (Deemed to be University), Mangalore, Karnataka, India
[2] Resident, Department of Orthodontics and Dentofacial Orthopaedics, Yenepoya Dental College, Yenepoya (Deemed to be University), Mangalore, Karnataka, India
[3] Associate Professor, Department of Orthodontics and Dentofacial Orthopaedics, Yenepoya Dental College, Yenepoya (Deemed to be University), Mangalore, Karnataka, India

***Corresponding author:** Dilshad Umar

Address: Department of Orthodontics and Dentofacial Orthopaedics, Yenepoya Dental College, University Road, Deralakatte, Mangaluru, Karnataka 575018, India

E-mail: orthodil@gmail.com

Received: 2026 April 08; **Revised:** 2026 May 07; **Accepted:** 2026 May 12

Abstract

Aim

To evaluate stress distribution and displacement patterns during infrazygomatic crest (IZC)–supported full-arch distalization with intrusion and to compare the biomechanical performance of single versus dual anterior temporary anchorage device (TAD) configurations using finite element analysis.

Methods

A CBCT-based three-dimensional finite element model of the maxillary dentoalveolar complex was constructed, including teeth, periodontal ligament (PDL), cortical and cancellous bone, archwire, IZC screws, and TADs. Two anchorage configurations were simulated: a single anterior TAD placed between the maxillary central incisors and dual anterior TADs placed bilaterally between the central and lateral incisors, both combined with IZC screws. Distalization forces ranging from 50 to 700 g were applied with a constant intrusive force of 50 g. Von Mises stress distribution and displacement patterns were evaluated in the cortical bone, PDL, dental roots, and anchorage components.

Results

Fourteen loading conditions (50–700 g distalization combined with 50 g intrusion) were analyzed. At low force levels (50–250 g), stresses remained within physiologic limits, with root stress ranging from 1.40 to 1.80 MPa and PDL stress from 0.015 to 0.020 MPa. With moderate forces (300–475 g), stresses increased, and root stress reached 2.88–3.03 MPa while PDL stress ranged from 0.026 to 0.030 MPa. At higher forces (500–700 g), stress levels further increased, with root stress ranging from 4.18 to 4.38 MPa and PDL stress from 0.041 to 0.044 MPa, indicating a potential overload region. Overall, stress and displacement values increased proportionally with increasing distalization force. The dual TAD configuration consistently demonstrated more favorable biomechanical behavior than the single-TAD model, showing lower stress concentrations in cortical bone and the periodontal ligament, more uniform stress distribution, and reduced displacement of the maxillary teeth.

Conclusion

Dual anterior TAD reinforcement during IZC-supported full-arch distalization with intrusion demonstrated a more uniform stress distribution and lower displacement values compared with the single TAD configuration, suggesting differences in biomechanical behavior between the two anchorage systems. Careful regulation of distalization force magnitude may help minimize localized stress within the dentoalveolar structures during skeletal anchorage–supported maxillary distalization.

Keywords: Finite element study, Full-arch distalization, Infrazygomatic crest, Intrusion, Temporary anchorage device.

Copyright © 2026, Author(s). This is an open-access article distributed under the terms of the Creative Commons Attribution-NonCommercial 4.0 International License (http://creativecommons.org/licenses/by-nc/4.0/) which permits copy and redistribute the material just in noncommercial usages, provided the original work is properly cited.

Background

Orthodontically induced root resorption (OIRR) is a well-recognized adverse effect of orthodontic tooth movement, characterized by the loss of cementum and, in severe cases, underlying dentin (1–4). Although typically mild and self-limiting, it assumes clinical significance when heavy or continuous forces are applied, particularly during complex movements such as full-arch distalization combined with intrusion (5–9). Understanding the biomechanical factors influencing OIRR is therefore essential for optimizing orthodontic force systems and minimizing adverse outcomes.

Temporary anchorage devices (TADs) have significantly expanded the scope of non-extraction orthodontic treatment by providing reliable skeletal anchorage independent of patient compliance. Among these, infrazygomatic crest (IZC) screws have gained prominence for full-arch distalization due to their placement in dense cortical bone, ability to withstand higher force levels, and minimal interference with tooth movement (10–16). However, the use of extra-alveolar anchorage systems often involves the application of relatively high forces, which may increase stress within the periodontal ligament (PDL) and root structure, thereby potentially elevating the side effects (17).

Full-arch distalization combined with intrusion is among the most biomechanically demanding orthodontic movements. The multidirectional force systems involved can result in non-uniform stress distribution across the root surfaces and supporting bone (18). Previous studies have emphasized the critical role of force magnitude, direction, and anchorage configuration in influencing stress concentration and the potential for root resorption (19). However, direct evaluation of internal stress distribution within the tooth–PDL–bone complex remains challenging with conventional clinical and radiographic methods.

The finite element method (FEM) provides a reliable computational approach for three-dimensional analysis of orthodontic biomechanics, enabling detailed assessment of stress distribution and displacement patterns that cannot be measured in vivo (20). Although FEM has been widely used to evaluate orthodontic tooth movement, most previous studies have focused on isolated tooth movement, posterior intrusion, incisor intrusion, segmental mechanics, or conventional mini-implant-supported distalization (21-23). Limited evidence is available regarding the distribution of OIRR-related stress during IZC-supported full-arch distalization combined with simultaneous intrusion, particularly when comparing single- and dual anterior TAD configurations. This represents an important knowledge gap because combined sagittal and vertical force systems may produce localized stress concentrations in the PDL and root surfaces, which are clinically relevant to root resorption risk.

Therefore, the present three-dimensional finite element study aimed to evaluate and compare stress distributions associated with OIRR risk during IZC-supported full-arch distalization with intrusion using single- and dual anterior TAD configurations. By identifying areas of localized periodontal and root stress, this study may help guide the selection of a clinically safer force system to better understand biomechanical stress patterns potentially associated with OIRR risk.

Methods

In this study, The model was reconstructed from the CBCT records of an adult patient with complete permanent dentition and no craniofacial abnormalities. The Young's modulus and Poisson's ratio values used in the model were as follows: tooth/dentin, 18,600 MPa and 0.31; periodontal ligament, 0.0689 MPa and 0.45; cortical bone, 13,700 MPa and 0.30; and cancellous bone, 1,370 MPa and 0.30, respectively. The stainless steel archwire was assigned a Young's modulus of 200,000 MPa and Poisson's ratio of 0.30, while the titanium TADs and IZC screws were assigned a Young's modulus of 110,000 MPa and Poisson's ratio of 0.35. The final mesh consisted of approximately 1.2–1.4 million nodes and 3.4–3.8 million tetrahedral elements, depending on the anchorage configuration

The CBCT data used for model construction were previously acquired as part of routine diagnostic records and anonymized prior to analysis. No additional radiographic exposure was performed specifically for this finite element study. The study was conducted in accordance with institutional ethical requirements for the use of retrospective anonymized imaging data (Ethical code: YEC2/2024/057).

Image segmentation was performed using Mimics software (Materialise NV, Leuven, Belgium), and the generated surfaces were refined and converted into solid models using 3-Matic software (Materialise NV, Leuven, Belgium). The PDL was modeled as a uniform 0.25 mm-thick layer surrounding the root surface. Material properties were assigned based on previously published literature (21).

The finalized geometric model was imported into ANSYS Workbench version 17.2 (ANSYS Inc., Canonsburg, PA, USA) for meshing and finite element analysis.

Tetrahedral elements were used for discretization, and mesh convergence testing was performed to ensure the accuracy and stability of the simulation results, with element size and node density optimized accordingly. Model validity was assessed qualitatively by comparing the observed stress concentration and displacement patterns with previously published orthodontic FEM studies involving TAD-supported intrusion, distalization, and mini-implant anchorage mechanics(10,14,20,24,26). The regions of peak stress observed in the present model, particularly around the implant neck, cortical bone, PDL, and apical/cervical root areas, were consistent with previously reported biomechanical patterns in orthodontic FEM and mini-implant anchorage studies (19).

Although direct experimental validation was not performed, this qualitative comparison was used to assess the plausibility of the simulation outputs. All materials were assumed to be homogeneous, isotropic, and linearly elastic, consistent with commonly adopted assumptions in finite element analyses of orthodontic biomechanics. These assumptions were applied to simplify the complex anisotropic behavior of biological tissues, improve computational stability, and enable standardized comparison with previous orthodontic FEM studies, while recognizing that they do not fully reproduce the nonlinear, patient-specific behavior of living tissues.

Two anterior anchorage configurations were evaluated: a single TAD placed in the midline between the maxillary central incisors, and dual TADs placed interradicularly between the maxillary central and lateral incisors bilaterally (Figure 1).

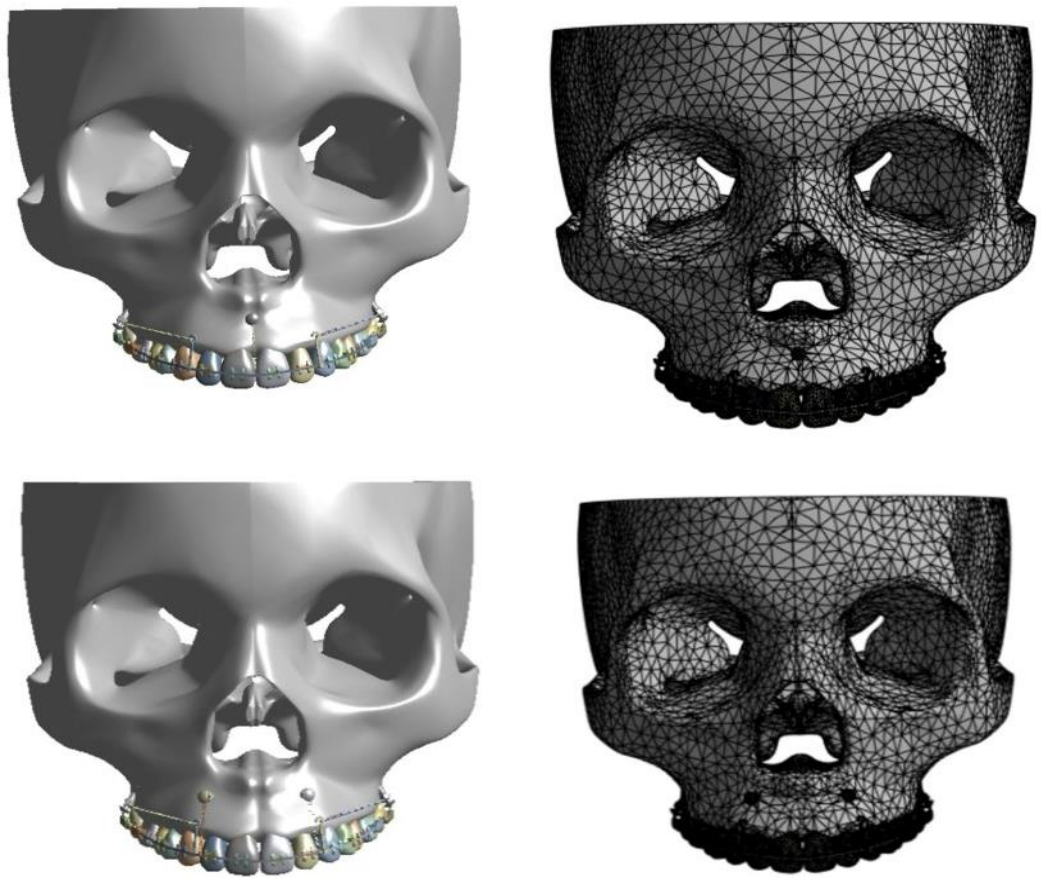

Figure 1. Schematic representation of anchorage configurations and force application.
(Upper) Single TAD configuration with a midline implant between maxillary central incisors
(Lower) Dual TAD configuration with bilateral interradicular implants.

In both configurations, an additional IZC screw was positioned in the infrazygomatic crest region to simulate full-arch distalization mechanics. Fourteen loading conditions were simulated, with horizontal distalization forces ranging from 50 g to 700 g in increments of 50 g. Higher force magnitudes were included to evaluate biomechanical behavior under potential overload conditions. In addition, a constant intrusive force of 50 g was applied in all simulations to replicate the vertical component of combined distalization and intrusion mechanics. The intrusive force was kept constant to isolate the biomechanical effect of progressively increasing distalization force while maintaining a standardized vertical force component across all simulations. This allowed comparison between single and dual TAD configurations without introducing additional variability from changes in the intrusive vector. Each loading condition was evaluated under both single and dual TAD configurations, yielding a total of 28 simulations. The applied force system, therefore, consisted of a horizontal distalization component and a vertical intrusive component. As the model was constructed symmetrically, no medio-lateral force component was applied, and the transverse force component was considered to be 0 g in all simulations. The distalization force range of 50–700 g was selected to simulate a broad spectrum of incremental orthodontic loading conditions, ranging from light force levels to higher force magnitudes that may be encountered during skeletal anchorage-supported full-arch distalization (24). This range enabled evaluation of force-dependent stress escalation and the identification of force levels at which localized PDL, root, and cortical bone stress, as well as anchorage stress, became more pronounced. The detailed distribution of force components across all loading conditions is presented in Table 1.

Specifically, nodes along the superior and posterior surfaces of the maxillary bone were fixed in all translational and rotational degrees of freedom to simulate craniofacial skeletal support and prevent rigid body displacement during loading. Tooth movement was permitted through deformation of the periodontal ligament, while the external boundaries of the maxillary model were constrained to maintain overall model stability. Adjacent teeth were modeled with frictionless surface-to-surface contact, and the archwire–bracket slot interface was defined as frictionless contact to simulate sliding mechanics during distalization, whereas the implant–bone interface was assumed to be bonded. The archwire was modeled as a rectangular stainless steel wire (0.019×0.025 inch), consistent with commonly used working archwires for sliding mechanics in orthodontic treatment. The primary outcome measures included von Mises stress distribution in the maxilla, cortical bone, periodontal ligament, IZC screw, and anterior TADs. Stress values were evaluated across the entire volume of each structure, and the maximum (peak) von Mises stress values were recorded for quantitative analysis. In addition, qualitative assessment of stress distribution patterns was performed using color-coded contour plots to identify regions of stress concentration.

Table 1. Applied loading protocol

Loading condition	Horizontal force (Distalization, g)	Vertical force (Intrusion, g)	Medio-lateral force (g)
1	50	50	0
2	100	50	0
3	150	50	0
4	200	50	0
5	250	50	0
6	300	50	0
7	350	50	0
8	400	50	0
9	450	50	0
10	500	50	0
11	550	50	0
12	600	50	0
13	650	50	0
14	700	50	0

Results

A total of 14 loading conditions were analyzed, with horizontal distalization forces ranging from 50 g to 700 g in 50 g increments while maintaining a constant 50 g intrusive force. Each loading condition was simulated for both single and dual anterior TAD configurations, resulting in 28 finite element simulations. Across all simulations, both stress magnitude and deformation increased proportionally with the applied distalization force; however, distinct biomechanical differences were observed between the two anchorage systems.

Stress distribution

The overall trend of stress distribution across increasing force levels is summarized in Table 2. At lower force magnitudes (50–250 g), root stress (1.40–1.80 MPa) and PDL stress (0.015–0.020 MPa) remained within a physiologic range. As the distalization force increased to 300–475 g, root stress increased to 2.88–3.03 MPa and PDL stress to 0.026–0.030 MPa, indicating increased compressive loading within the periodontal structures. At higher force magnitudes (500–700 g), root stress reached 4.18–4.38 MPa and PDL stress approached 0.041–0.044 MPa, corresponding to a high-stress region associated with potential biologic overload. In the single TAD configuration, increasing force magnitude resulted in progressive stress amplification with localized concentration in the anterior maxillary cortical bone, midline anchorage region, and implant neck. Figure 2 illustrates the von Mises stress distribution in the maxillary bone, demonstrating focal stress accumulation around the IZC screw and adjacent cortical structures. In contrast, the dual TAD configuration exhibited a more homogeneous stress distribution across the maxilla and anchorage system. The use of two anterior TADs facilitated improved load sharing, reducing localized peak stresses around the IZC anchorage area and anterior maxillary cortical bone.

Tooth displacement patterns

Both anterior and posterior teeth exhibited increasing distal displacement with increasing force magnitude; however, the magnitude and pattern of movement differed between anchorage systems (Table 3). The single TAD model demonstrated greater overall displacement (0.52–0.78 mm) and a progressive tendency toward tipping as force levels increased.

Figure 3 illustrates the displacement patterns and stress distribution in the PDL, anterior and posterior dentition, and peri-IZC region for single and dual TAD configurations. In the single TAD model, greater anterior deformation was observed, reaching approximately 7.89×10^{-4} mm, with displacement vectors indicating a noticeable tipping tendency of the anterior teeth. Posterior deformation also reached about 6.26×10^{-4} mm, suggesting reduced anchorage control. In contrast, the dual TAD configuration showed lower anterior displacement ($\approx6.75\times10^{-4}$ mm) and posterior deformation ($\approx4.75\times10^{-4}$ mm), indicating improved anchorage stability and more controlled bodily tooth movement. Additionally, peri-IZC stress decreased from approximately 4.3757 MPa in the single TAD model to 4.1836 MPa in the dual TAD model. PDL stress distribution was also more uniform in the dual TAD configuration, reflecting improved biomechanical load sharing.

High-load biomechanical comparison

The most pronounced differences between the two anchorage systems were observed at higher distalization forces (>300–400 g). Under the 600 g loading condition, the dual TAD configuration demonstrated reduced peak stress and improved displacement control compared with the single TAD model (Table 4). Specifically, the dual TAD system exhibited a 4.4% reduction in maximum cortical bone stress, a 6.7% reduction in maximum PDL stress, and a 12.3% reduction in anterior tooth displacement. Posterior displacement values were also consistently lower in the dual TAD configuration, indicating improved anchorage stability and more controlled force transmission. Detailed ANSYS output parameters for the 600 g loading condition are provided in Table 5.

Table 2. Stress distribution across distalization force levels (50–700 g)

Force Range (g)	Root Stress (MPa)	PDL Stress (MPa)	Interpretation
50–250	1.40–1.80	0.015–0.020	Physiologic stress range
300–475	2.88–3.03	0.026–0.030	Increased compressive loading
500–700	4.18–4.38	0.041–0.044	Saturation of PDL stress (high risk zone)

Table 3. Comparison of displacement between anchorage systems

Parameter	Single TAD	Dual TAD	Interpretation
Maximum displacement (mm)	0.52–0.78	0.37–0.51	Higher displacement in single TAD
High force displacement (mm)	0.77–0.78	0.38–0.50	Better control in dual TAD

Table 4: Comparative biomechanical response at the 600-g load condition

Parameter	Single TAD (Mpa)	Dual TAD (Mpa)	Comparative change
Max cortical bone stress at 600 g (MPa)	4.3798	4.1871	↓ 4.4%
Max PDL stress at 600 g (MPa)	0.043875	0.040954	↓ 6.7%
Max IZC stress at 600 g (MPa)	4.3798	4.1871	↓ 4.4%
Anterior displacement at 600 g (mm)	9.04×10^{-4}	7.93×10^{-4}	↓ 12.3%
Posterior displacement at 600 g (mm)	$2.96–7.08\times10^{-4}$	$2.34–4.75\times10^{-4}$	Reduced

Table 5. Detailed ANSYS output (600-g case)

Parameter	Single TAD	Dual TAD
Max cortical bone stress (MPa)	4.3798	4.1871
Max PDL stress (MPa)	0.043875	0.040954
Max IZC stress (MPa)	4.3798	4.1871
Anterior displacement (mm)	9.04×10^{-4}	7.93×10^{-4}
Posterior displacement (mm)	$2.96–7.08\times10^{-4}$	$2.34–4.75\times10^{-4}$

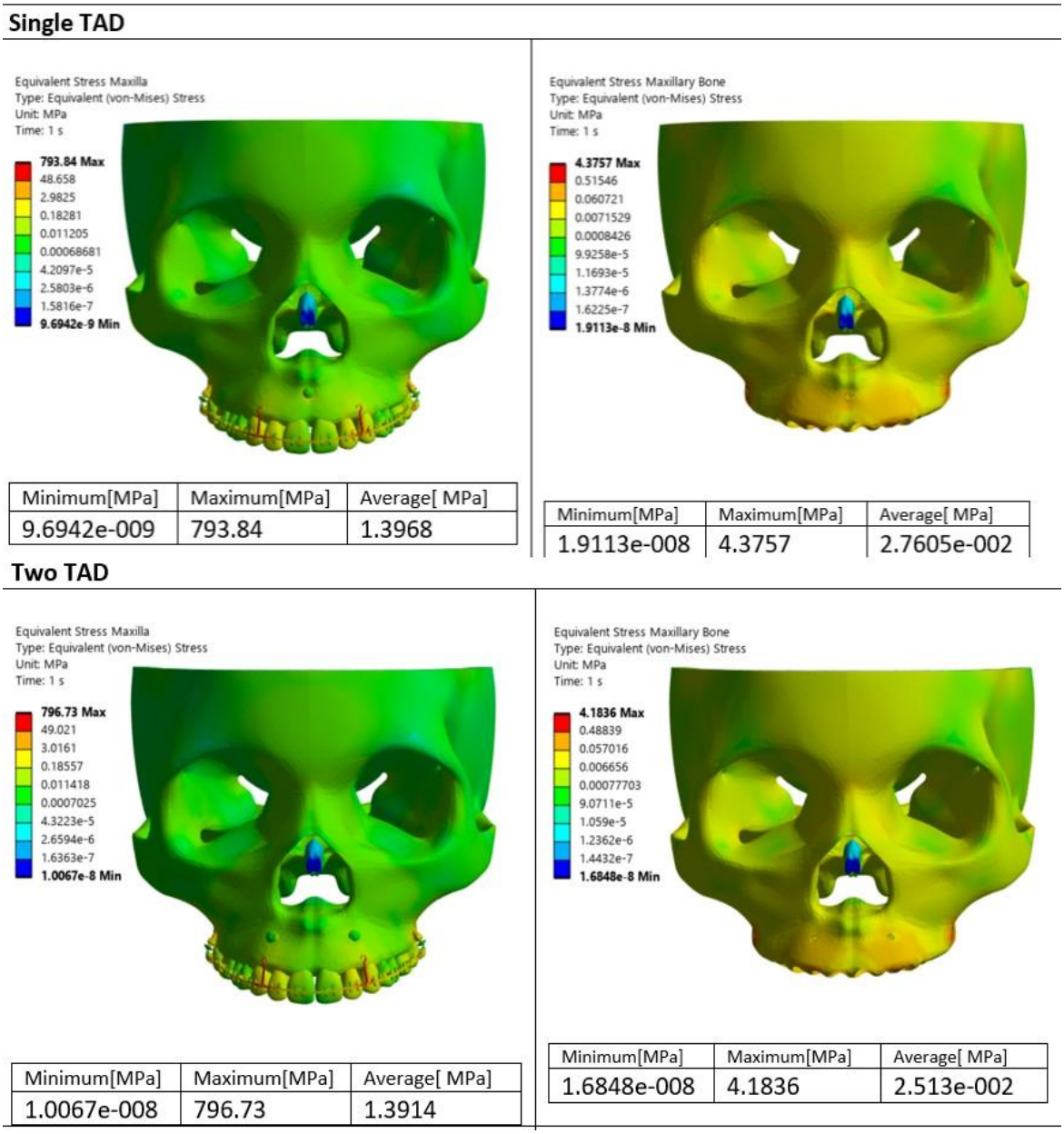

Figure 2. Von Mises stress distribution in the maxillary bone under 600-g distalization force with 50-g intrusion comparing single and dual anterior TAD configurations.
Upper panels: Single-TAD anchorage shows higher localized stress concentration around the IZC anchorage region and anterior maxillary cortical bone, reflecting reduced load sharing.
Lower panels: The dual TADs anchorage configuration demonstrates a more uniform stress distribution with reduced peak concentrations along the IZC and anterior buttress regions, indicating improved biomechanical control and load dispersion.
Color scale represents equivalent stress (MPa), where warmer colors denote higher stress.

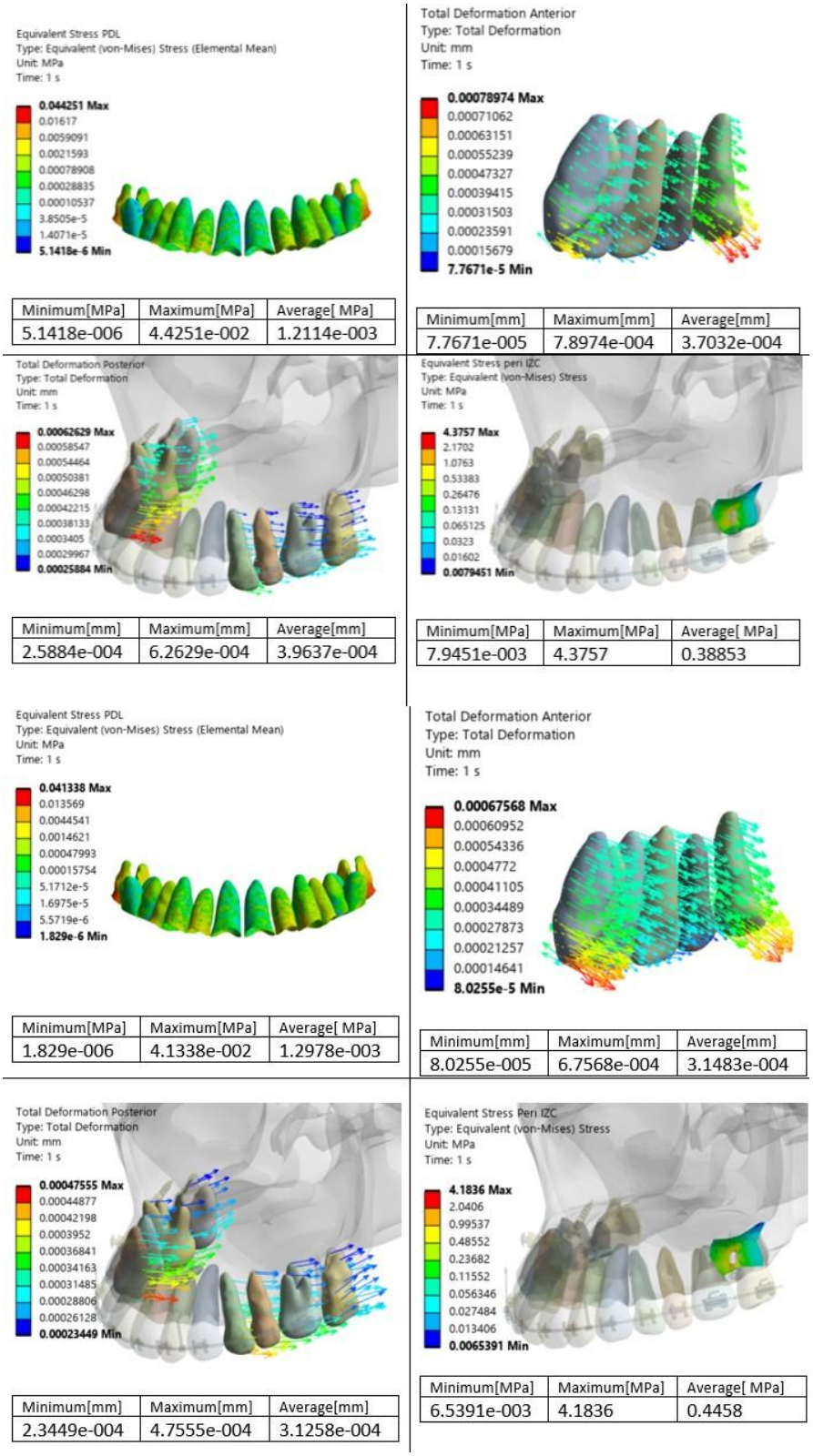

Figure 3. Comparison of periodontal ligament stress, dental displacement, and anchorage stress in single and dual anterior TAD configurations. Two upper panels show the single-TAD model and two lower panels the dual-TAD model. The single-TAD configuration exhibits higher localized PDL stress, greater anterior displacement, and increased peri-IZC stress, whereas the dual-TAD configuration demonstrates more uniform stress distribution, reduced displacement, and improved load sharing. Warmer colors indicate higher stress or deformation.

Discussion

Orthodontically induced root resorption (OIRR) is a multifactorial biological process influenced by the magnitude, direction, and duration of orthodontic forces (25). The present study evaluated the biomechanical behavior of the maxillary dentoalveolar complex during full arch distalization with intrusion using single and dual TAD configurations supported by infrazygomatic crest (IZC) screws. Unlike previous FEM studies that primarily assessed isolated or segmental orthodontic mechanics, this study evaluated a combined full arch distalization-intrusion force system and compared the biomechanical effects of single versus dual anterior TAD reinforcement under progressively increasing distalization forces. Compared with previous FEM studies that evaluated isolated intrusion, posterior intrusion, or segmental distalization, the present model provides additional insight into how combined sagittal and vertical force vectors may influence stress distribution across the full maxillary arch. A force-dependent increase in stress and deformation was observed across all simulations, highlighting the critical role of force magnitude in determining biomechanical response.

The progressive increase in cortical and maxillary stress reinforces the biomechanical sensitivity of skeletal anchorage-supported distalization to force magnitude. Cortical bone consistently exhibited the highest stress concentrations, particularly at the implant neck–bone interface. This finding is consistent with previous biomechanical studies emphasizing the importance of cortical bone in determining mini-implant stability (26). The marked increase in cortical stress at higher force levels suggests a potential risk of overload, which may compromise anchorage stability under excessive distalization forces.

A key finding of this study was the more favorable stress distribution observed in the dual TAD configuration. In contrast to the single TAD model, which demonstrated localized stress concentration in the anterior maxilla and midline anchorage region, the dual TAD system exhibited more uniform load distribution with reduced peak stress values. This observation reflects the principle of load sharing, whereby multiple anchorage units distribute applied forces more effectively, thereby minimizing stress concentration at individual sites. Similar findings have been reported in finite element analyses of reinforced skeletal anchorage systems (27).

Biomechanically, the advantage of the dual TAD configuration may be explained by distribution of the applied load across two anterior anchorage units rather than concentration at a single midline point. This load-sharing effect likely reduces localized stress at the implant neck and adjacent cortical bone while improving control over anterior tooth displacement. Clinically, this suggests that dual anterior reinforcement may be particularly useful when higher distalization forces are required, although the decision to use additional TADs should also consider anatomical limitations, patient comfort, soft-tissue tolerance, and operator preference.

The periodontal ligament (PDL) response is central to understanding the risk of OIRR. From a biological perspective, the lower and more homogeneous PDL stress pattern observed with dual TAD anchorage may be relevant because concentrated compressive stresses are considered important contributors to hyalinization and subsequent resorptive activity. Concentrated PDL stress has been associated with hyalinization and subsequent external apical root resorption(28). Therefore, the more uniform stress distribution observed in the dual TAD model may indicate a reduced theoretical risk of root resorption, particularly under higher force conditions.

Tooth displacement patterns further supported these findings. The improved displacement control observed with dual TAD anchorage can be explained by a more balanced force system and reduced rotational tendency of the anterior segment. Previous studies have shown that uncontrolled tipping results in greater stress concentration in cervical and apical regions, thereby increasing the susceptibility to resorptive changes(29). Similarly, posterior tooth movement in the dual TAD system was better controlled, with reduced tipping compared to the single TAD model, indicating more controlled biomechanical response.

deterministic analysThe behavior of the IZC screw is of particular clinical relevance in full arch distalization mechanics. In the present study, stress in the IZC screw increased with force magnitude in both configurations; however, stress levels were consistently higher in the single TAD system. The dual TAD configuration reduced the load borne by the IZC screw through effective force distribution. Although IZC screws are known for their high stability due to engagement with dense cortical bone, excessive stress may increase the risk of micromovement or anchorage failure.[27,28] These

findings underscore the importance of anchorage design in optimizing biomechanical performance. However, the choice between single and dual TAD mechanics in clinical practice is not determined by biomechanical findings alone. Other factors such as ease of placement, anatomical constraints, soft-tissue tolerance, anchorage stability, patient comfort, and operator preference should also be considered when selecting the most appropriate force application method.

From a clinical standpoint, the results emphasize the importance of force magnitude control during full arch distalization. While physiologic stress patterns were observed at lower force levels, forces exceeding approximately 300–400 g resulted in marked increases in cortical, PDL, and implant stresses. This observation is consistent with biological evidence indicating that heavier continuous forces are associated with increased risk of periodontal hyalinization and root resorption (31-33). Therefore, careful calibration of force magnitude remains essential, even when skeletal anchorage systems are employed.

Clinically, the findings suggest that lower to moderate distalization forces may be preferable when the objective is to minimize localized PDL and root stress during IZC-supported full arch distalization with intrusion. When higher force magnitudes are required, dual anterior TAD reinforcement may offer a more favorable anchorage strategy by distributing loads more evenly and reducing focal stress concentration at the anterior anchorage units and IZC screw. However, these recommendations should be interpreted cautiously, as FEM findings represent initial biomechanical responses and must be individualized according to root morphology, periodontal status, bone quality, anatomical limitations, and patient-specific treatment objectives.

The limitations of this study are inherent to finite element analysis. The model assumed homogeneous, isotropic, and linearly elastic material properties, which may not fully replicate the complex anisotropic and nonlinear behavior of biological tissues. Patient-specific variability in root morphology, periodontal ligament thickness, cortical bone density, alveolar bone quality, and skeletal anatomy was not incorporated. Additionally, static loading conditions were applied, and time-dependent biological responses such as bone remodeling, periodontal adaptation, hyalinization, and root resorption progression were not simulated. Simplified contact assumptions, including frictionless tooth–tooth and archwire bracket interactions and a perfectly bonded implant–bone interface, may not fully represent clinical conditions. In addition, direct experimental or clinical validation of the FEM model was not performed; however, the stress distribution and displacement patterns were qualitatively consistent with previously published orthodontic FEM studies. As this was a deterministic FEM study, formal statistical testing and probabilistic sensitivity analysis were not performed. However, comparative percentage differences between anchorage configurations and force-dependent trends across incremental loading conditions were evaluated to improve interpretation of the biomechanical response. Future studies incorporating patient-specific models, nonlinear material properties, time-dependent loading conditions, experimental validation, and clinical correlation may provide more clinically representative insights.

The findings of the present study demonstrate that increasing distalization force results in a corresponding increase in stress within the dentoalveolar complex. Furthermore, the dual TAD configuration provides a more favorable biomechanical environment by improving stress distribution, reducing peak stress concentrations, and enhancing control of tooth movement. These findings have important clinical implications for minimizing the risk of OIRR during IZC-supported full arch distalization with intrusion

Limitations

This study has several limitations inherent to finite element analysis. The materials were assumed to be homogeneous, isotropic, and linearly elastic, which does not fully represent the complex anisotropic and nonlinear behavior of biological tissues. Patient-specific variations in root morphology, periodontal ligament thickness, cortical bone density, alveolar bone quality, and skeletal anatomy were not incorporated into the model. Static loading conditions were applied, and time-dependent biological processes such as bone remodeling, periodontal ligament adaptation, hyalinization, and progressive root resorption could not be simulated. In addition, contact conditions were simplified, including frictionless tooth–tooth and bracket–archwire interactions, as well as a perfectly bonded implant–bone interface, which may differ from clinical reality. Direct experimental or clinical validation of the finite element model was not performed. Although the observed stress

distribution and displacement patterns were qualitatively consistent with previously published orthodontic finite element studies, the results should be interpreted as representing initial biomechanical responses rather than definitive clinical outcomes. Future studies incorporating patient-specific models, nonlinear material properties, dynamic loading conditions, and clinical validation are warranted.

Conclusion

Within the limitations of this finite element study, increasing distalization force was associated with increased stress within the maxillary dentoalveolar complex during IZC-supported full-arch distalization with intrusion. Higher force magnitudes produced greater stress concentrations in the cortical bone, periodontal ligament, and anchorage components. Under the conditions of the present simulation, the dual TAD configuration demonstrated a somewhat more uniform stress distribution and lower displacement values compared with the single TAD model. These findings may indicate a difference in biomechanical behavior between the two anchorage designs; however, the clinical significance of these differences cannot be determined from finite element analysis alone. Because the present study was based on simplified material assumptions and static loading conditions, the results should be interpreted cautiously and considered representative of simulated biomechanical patterns rather than direct clinical outcomes.

Acknowledgments

None.

Conflicts of Interest

The authors do not have any competing interests to declare.

Data availability statements

The data supporting the findings of this study are available from the corresponding author upon reasonable request.

Funding

None.

References

1. Brezniak N, Wasserstein A. Root resorption after orthodontic treatment: Part 1. Literature review. Am J Orthod Dentofacial Orthop. 1993;103(1):62-6. doi: 10.1016/0889-5406(93)70106-X.
2. Brezniak N, Wasserstein A. Orthodontically induced inflammatory root resorption. Part II: The clinical aspects. Angle Orthod. 2002;72(2):180-4. doi: 10.1043/0003-3219(2002)072<0180:OIIRRP>2.0.CO;2.
3. Samandara A, Papageorgiou SN, Ioannidou-Marathiotou I, Kavvadia-Tsatala S, Papadopoulos MA. Evaluation of orthodontically induced external root resorption following orthodontic treatment using cone beam computed tomography (CBCT): a systematic review and meta-analysis. Eur J Orthod. 2019;41(1):67-79. doi: 10.1093/ejo/cjy027.
4. Yassir YA, McIntyre GT, Bearn DR. Orthodontic treatment and root resorption: an overview of systematic reviews. Eur J Orthod. 2021;43(4):442-456. doi: 10.1093/ejo/cjaa058.
5. Weltman B, Vig KW, Fields HW, Shanker S, Kaizar EE. Root resorption associated with orthodontic tooth movement: a systematic review. Am J Orthod Dentofacial Orthop. 2010;137(4):462-76; discussion 12A. doi: 10.1016/j.ajodo.2009.06.021.
6. Bellini-Pereira SA, Almeida J, Aliaga-Del Castillo A, Dos Santos CCO, Henriques JFC, Janson G. Evaluation of root resorption following orthodontic intrusion: a systematic review and meta-analysis. Eur J Orthod. 2021;43(4):432-441. doi: 10.1093/ejo/cjaa054.
7. Huang TTY, Elekdag-Turk S, Dalci O, Almuzian M, Karadeniz EI, Gonzales C, Petocz P, Turk T, Darendeliler MA. The extent of root resorption and tooth movement following the application of ascending and descending magnetic forces: a prospective split-mouth, microcomputed-tomography study. Eur J Orthod. 2017;39(5):547-553. doi: 10.1093/ejo/cjw073.
8. Antonarakis GS, Zekeridou A, Kiliaridis S, Giannopoulou C. Periodontal considerations during orthodontic intrusion and extrusion in healthy and reduced periodontium. Periodontol 2000. 2024. doi: 10.1111/prd.12578.
9. Roscoe MG, Meira JB, Cattaneo PM. Association of orthodontic force system and root resorption: A systematic review. Am J Orthod Dentofacial Orthop. 2015;147(5):610-26. doi: 10.1016/j.ajodo.2014.12.026.
10. Schwertner A, de Almeida-Pedrin RR, Poleti TMFF, Oltramari P, de Castro Conti ACF, Cotrim-Ferreira FA, de Almeida G, Flores-Mir C, de Almeida MR. Biomechanical analysis of total arch maxillary distalization using infrazygomatic crest miniscrews: a finite element analysis study. Prog Orthod. 2024;25(1):10. doi: 10.1186/s40510-024-00509-3.
11. de Almeida MR. Clinical considerations for total arch distalization using extra-alveolar mini screws – An overview. Semin Orthod .2025;32(3): 557-567 .doi: 10.1053/j.sodo.2025.07.005

12. Ghosh A. Infra-zygomatic crest and buccal shelf-orthodontic bone screws: a leap ahead of micro-implants-clinical perspectives. J Indian Orthod Soc 2018;52(4 Suppl 2):127-141.doi: 10.4103/jios.jios_229_18.
13. Alkadhimi A. Distalization with extra-alveolar temporary anchorage devices in the infrazygomatic crest region. Orthod Update 2025;18(3):115-124.doi: 10.12968/ortu.2025.18.3.115.
14. Rosa WGN, de Almeida-Pedrin RR, Oltramari PVP, de Castro Conti ACF, Poleti TMFF, Shroff B, de Almeida MR. Total arch maxillary distalization using infrazygomatic crest miniscrews in the treatment of Class II malocclusion: a prospective study. Angle Orthod. 2023 ;93(1):41-48. doi: 10.2319/050122-326.1.
15. Shaikh A, Jamdar AF, Galgali SA, Patil S, Patel I, Hemagiriyappa MS. Efficacy of Infrazygomatic Crest Implants for Full-arch Distalization of Maxilla and Reduction of Gummy Smile in Class II Malocclusion. J Contemp Dent Pract. 2021;22(10):1135-1143.
16. Wu X, Liu H, Luo C, Li Y, Ding Y. Three-Dimensional Evaluation on the Effect of Maxillary Dentition Distalization With Miniscrews Implanted in the Infrazygomatic Crest. Implant Dent. 2018;27(1):22-27. doi: 10.1097/ID.0000000000000706.
17. Papadopoulos MA, Tarawneh F. The use of miniscrew implants for temporary skeletal anchorage in orthodontics: a comprehensive review. Oral Surg Oral Med Oral Pathol Oral Radiol Endod. 2007;103(5):e6-15. doi: 10.1016/j.tripleo.2006.11.022.
18. Liou EJ, Pai BC, Lin JC. Do miniscrews remain stationary under orthodontic forces? Am J Orthod Dentofacial Orthop. 2004;126(1):42-7. doi: 10.1016/j.ajodo.2003.06.018.
19. Motoyoshi M, Hirabayashi M, Uemura M, Shimizu N. Recommended placement torque when tightening an orthodontic mini-implant. Clin Oral Implants Res. 2006;17(1):109-14. doi: 10.1111/j.1600-0501.2005.01211.x.
20. Moss ML, Skalak R, Patel H, Sen K, Moss-Salentijn L, Shinozuka M, Vilmann H. Finite element method modeling of craniofacial growth. Am J Orthod. 1985;87(6):453-72. doi: 10.1016/0002-9416(85)90084-3.
21. Khosravi S, Jahanshad H, Moafi M, Shahmohamadi M, Kachoei M. Miniscrew placement on mandibular buccal shelf and infra-zygomatic crest area: A finite element analysis. J Adv Periodontol Implant Dent. 2025 ;17(4):205-215. doi: 10.34172/japid.025.3687.
22. Oğuz F, Özden S. Finite element analysis of maxillary arch distalization using skeletal anchorage at three different application regions. Sci Rep. 2025 ;15(1):24073. doi: 10.1038/s41598-025-10035-9.
23. Fares M, Marzouk W, Ismail HA, Abuouf Y, Kassem HE. Effect of multiple hook heights and positions during en masse maxillary distalization using infrazygomatic crest miniscrew- single and double points of force application: a finite element analysis study. BMC Oral Health. 2025 ;25(1):771. doi: 10.1186/s12903-025-06138-4.
24. Tanne K, Sakuda M, Burstone CJ. Three-dimensional finite element analysis for stress in the periodontal tissue by orthodontic forces. Am J Orthod Dentofacial Orthop. 1987;92(6):499-505. doi: 10.1016/0889-5406(87)90232-0.
25. Melsen B. Tissue reaction to orthodontic tooth movement--a new paradigm. Eur J Orthod. 2001;23(6):671-81. doi: 10.1093/ejo/23.6.671.
26. Cattaneo PM, Dalstra M, Melsen B. The finite element method: a tool to study orthodontic tooth movement. J Dent Res. 2005;84(5):428-33. doi: 10.1177/154405910508400506.
27. Kravitz ND, Kusnoto B. Risks and complications of orthodontic miniscrews. Am J Orthod Dentofacial Orthop. 2007;131(4 Suppl):S43-51. doi: 10.1016/j.ajodo.2006.04.027.
28. Wilmes B, Drescher D. Impact of insertion depth and predrilling diameter on primary stability of orthodontic mini-implants. Angle Orthod. 2009;79(4):609-14. doi: 10.2319/071708-373.1.
29. Lee JS, Kim DH, Park YC, Kyung SH, Kim TK. The efficient use of midpalatal miniscrew implants. Angle Orthod. 2004;74(5):711-4. doi: 10.1043/0003-3219(2004)074<0711:TEUOMM>2.0.CO;2.
30. Chan E, Darendeliler MA. Physical properties of root cementum: Part 5. Volumetric analysis of root resorption craters after application of light and heavy orthodontic forces. Am J Orthod Dentofacial Orthop. 2005;127(2):186-95. doi: 10.1016/j.ajodo.2003.11.026.
31. Cattaneo PM, Dalstra M, Melsen B. Strains in periodontal ligament and alveolar bone associated with orthodontic tooth movement analyzed by finite element. Orthod Craniofac Res. 2009;12(2):120-8. doi: 10.1111/j.1601-6343.2009.01445.x.
32. Liou EJ, Chen PH, Wang YC, Lin JC. A computed tomographic image study on the thickness of the infrazygomatic crest of the maxilla and its clinical implications for miniscrew insertion. Am J Orthod Dentofacial Orthop. 2007;131(3):352-6. doi: 10.1016/j.ajodo.2005.04.044.
33. Paetyangkul A, Türk T, Elekdağ-Türk S, Jones AS, Petocz P, Darendeliler MA. Physical properties of root cementum: part 14. The amount of root resorption after force application for 12 weeks on maxillary and mandibular premolars: a microcomputed-tomography study. Am J Orthod Dentofacial Orthop. 2009;136(4):492.e1-9; discussion 492-3. doi: 10.1016/j.ajodo.2009.03.008.